Supplementary Information

Blocking Polysulfide with Janus Fe_3C/N-CNF@RGO Electrode via Physiochemical Confinement and Catalytic Conversion for High-Performance Lithium-Sulfur Battery

Jiayi Li[a], Hongwei Zhang[a], Linqu Luo[a], Hao Li[a], Junyu He[a], Hongliang Zu[a], Lei Liu[b], Hao Liu[c], Fengyun Wang*[a] and Jianjun Song*[a]

[a] *College of Physics and State Key Laboratory of Bio-Textiles, Qingdao University, Qingdao 266071, China; Email: fywang@qdu.edu.cn; jianjun.song@qdu.edu.cn.*

[b] *School of Materials Science and Engineering, Shandong University of Science and Technology, Qingdao 266590, P.R China*

[c] *Centre for Clean Energy Technology, School of Mathematical and Physical Sciences, Faculty of Science, University of Technology Sydney, Broadway, Sydney, NSW 2007, Australia*

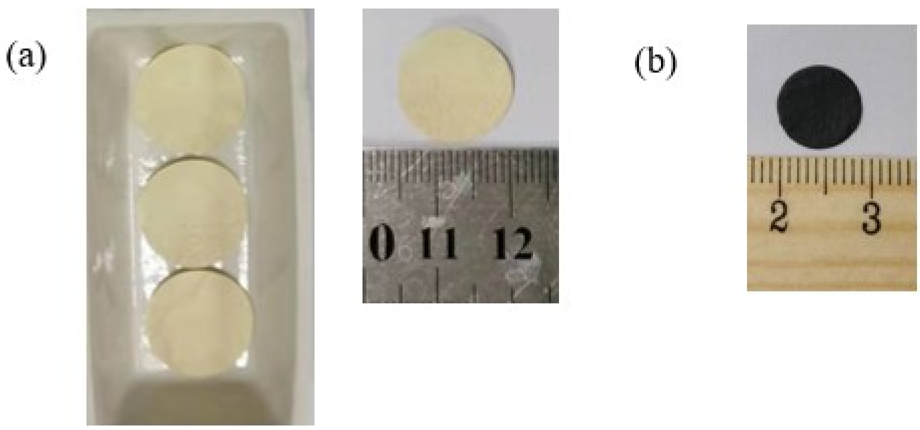

Fig. S1 Photograph of electrospun membranes (a) before and (b) after carbonation.

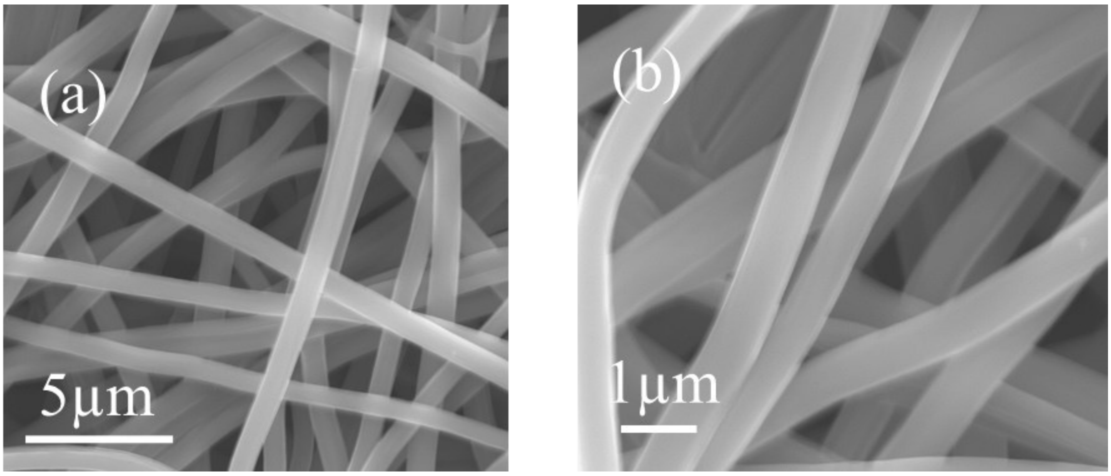

Fig. S2 (a) Low-magnification SEM image and (b) high-magnification SEM image of Fe_3C/N-CNF-0.3.

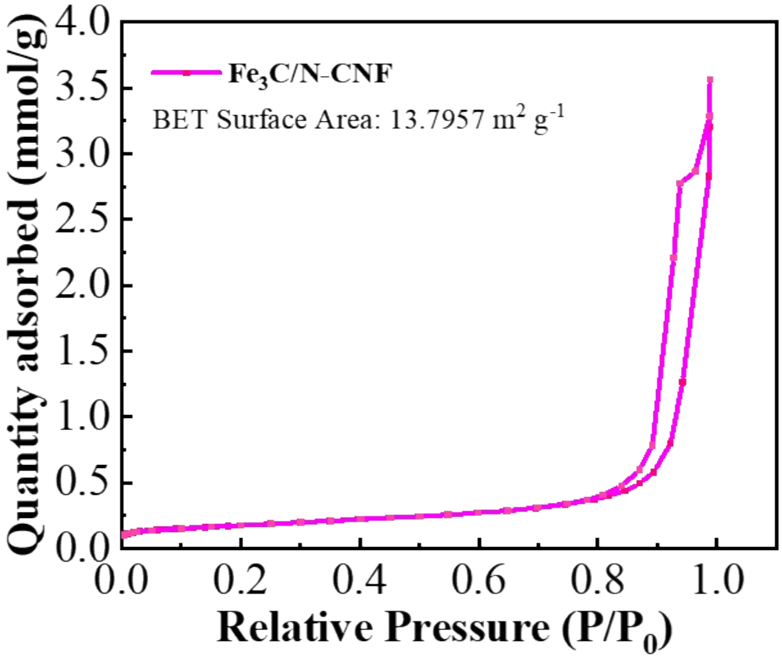

Fig. S3 N_2 adsorption-desorption isotherms of the Fe_3C/N-CNF.

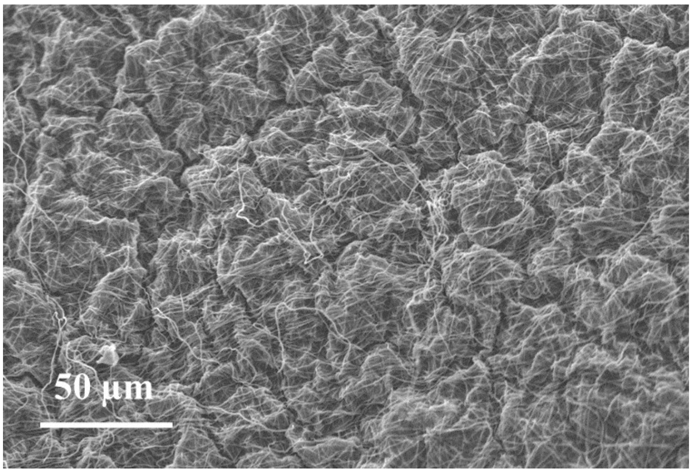

Fig. S4 Low-magnification SEM image of Fe_3C/N-CNF@RGO-0.2 electrode.

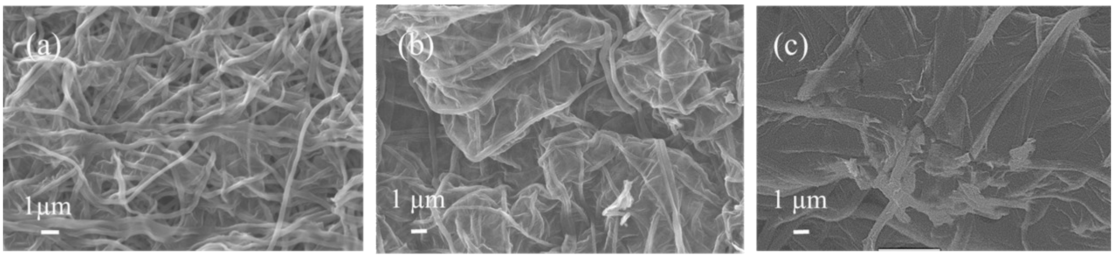

Fig. S5 SEM images of (a) Fe_3C/N-CNF@RGO-0.1, (b) Fe_3C/N-CNF@RGO-0.2, and (c) Fe_3C/N-CNF@RGO-0.4.

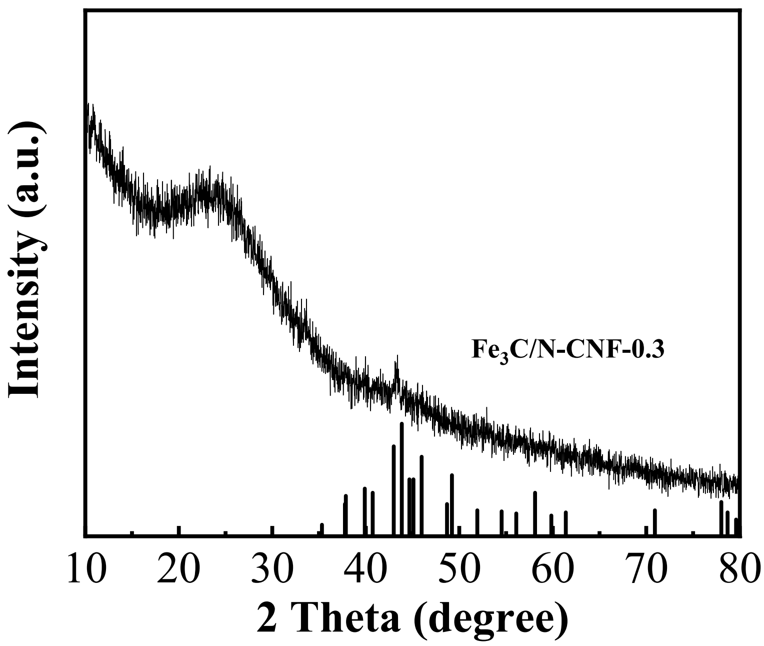

Fig. S6 XRD of the Fe_3C/N-CNF-0.3 electrode.

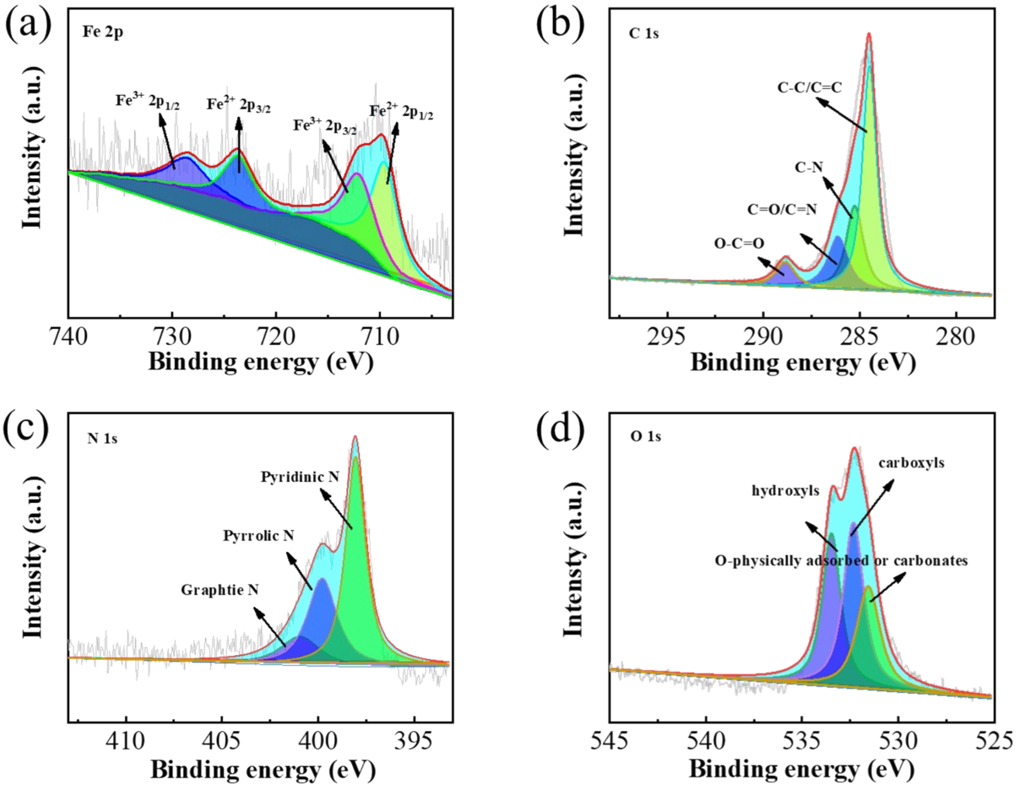

Fig. S7 High-resolution XPS spectra of (a) Fe 2p, (b) C 1s, (c) N 1s, and (d) O 1s for Fe_3C/N-CNF-0.3 composites.

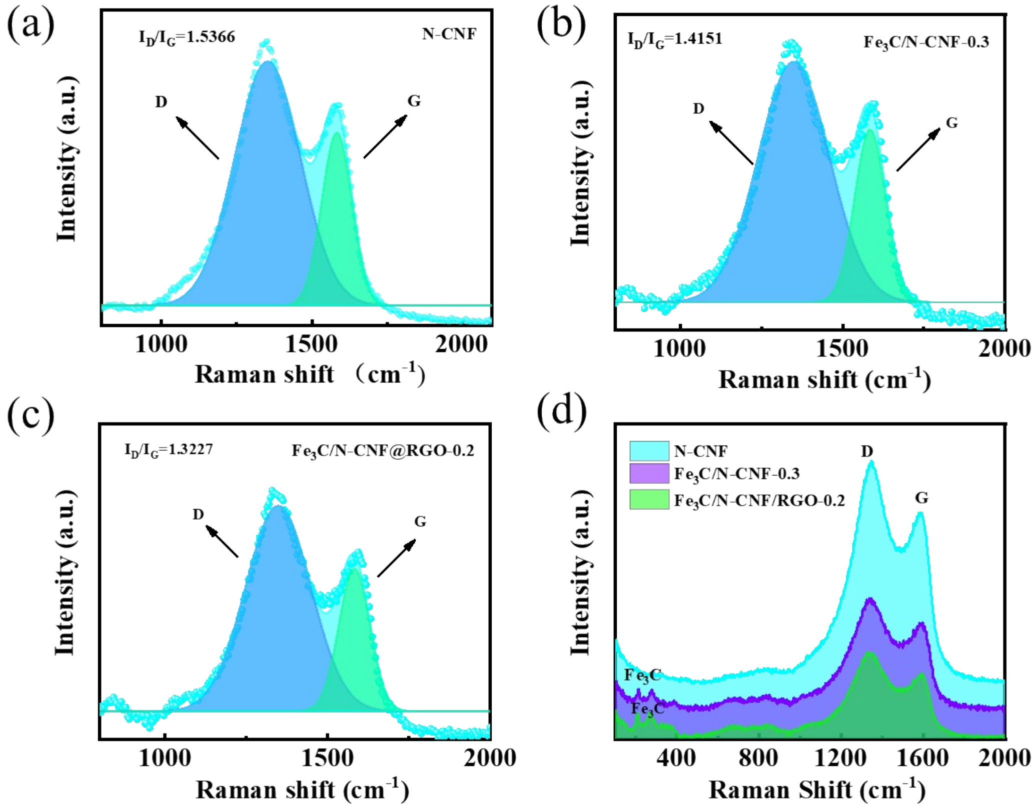

Fig. S8 The Raman spectra of (a) N-CNF, (b) Fe_3C/N-CNF-0.3, (c) Fe_3C/N-CNF@RGO-0.2 and (d) Direct comparison of Raman spectra.

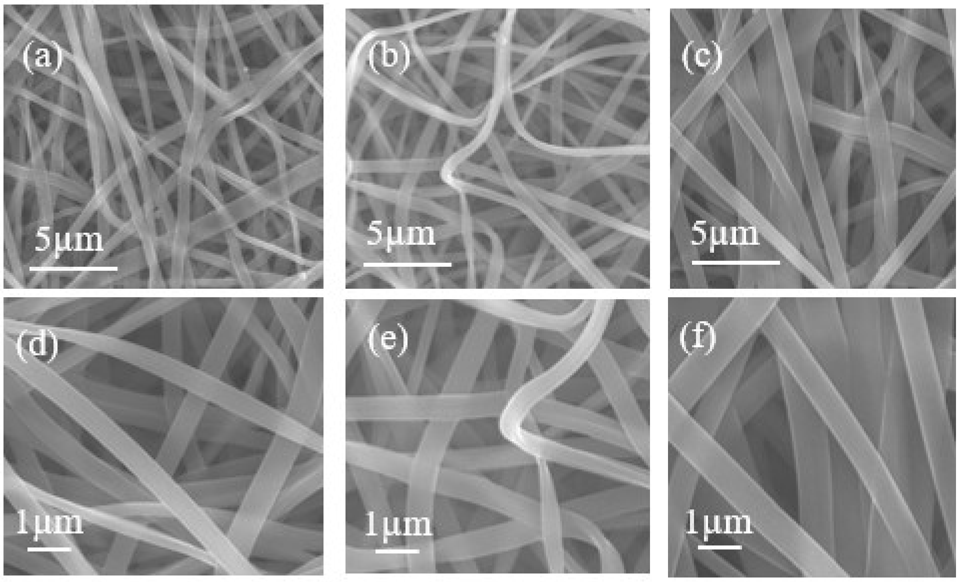

Fig. S9 Low-magnification SEM images of (a) N-CNF (b) Fe_3C/N-CNF-0.2, (c) Fe_3C/N-CNF-0.4 and high-magnification SEM images of (d) N-CNF (e) Fe_3C/N-CNF-0.2 and (f) Fe_3C/N-CNF-0.4.

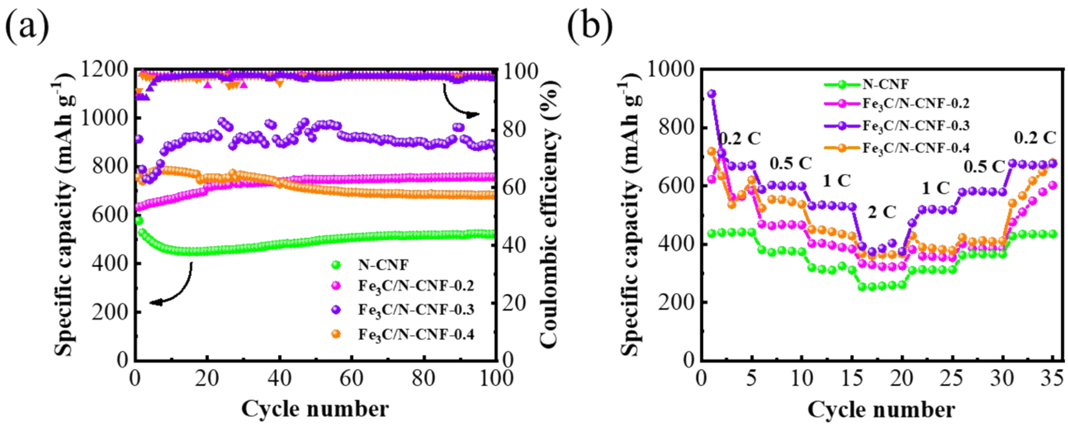

Fig. S10 (a) Cycling performance and (b) rate capabilities of LSBs with N-CNF， Fe_3C/N-CNF-0.2， Fe_3C/N-CNF-0.3 and Fe_3C/N-CNF-0.4 at 0.2 C for 100 cycles , and corresponding Coulombic efficiency.

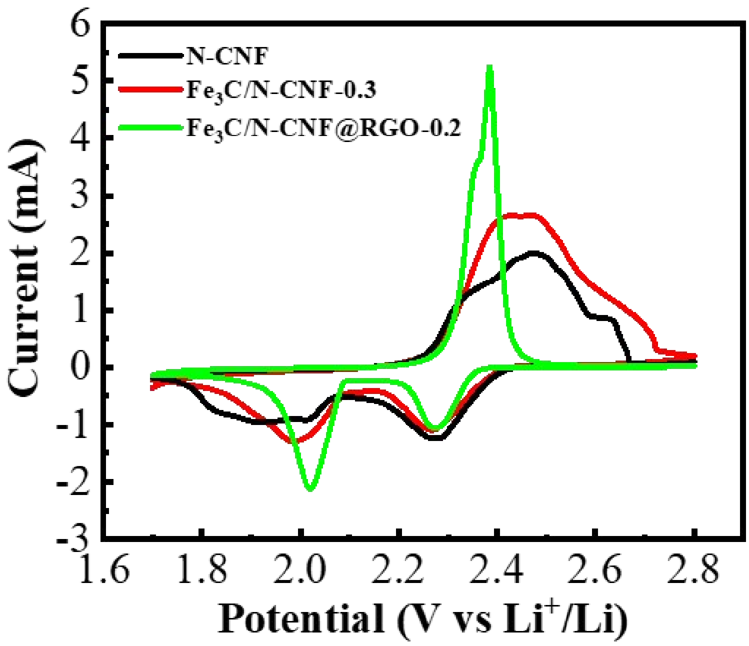

Fig. S11 The CV curves of first cycle of three cells with N-CNF, Fe_3C/N-CNF-0.3 and Fe_3C/N-CNF@RGO-0.2 electrodes.

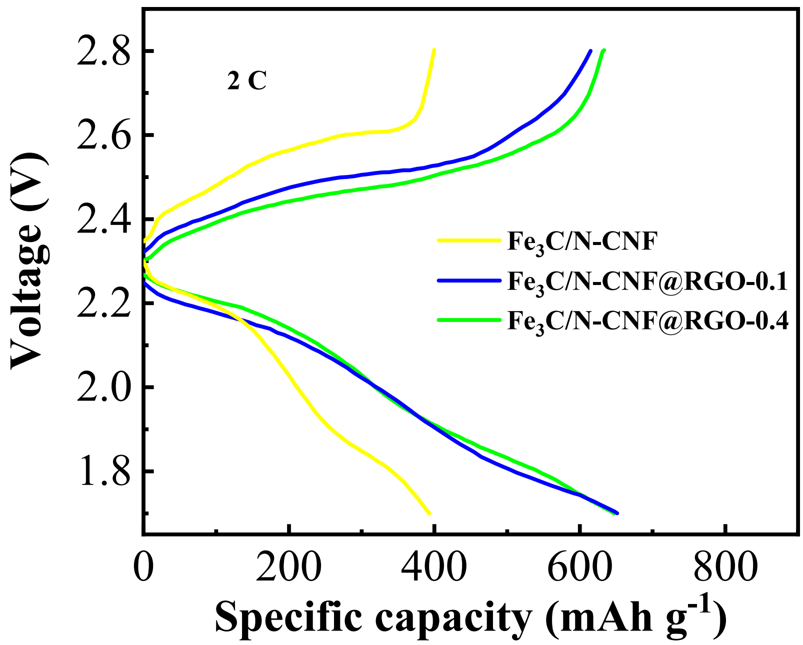

Fig. S12 Charge/discharge curves of Fe_3C/N-CNF, Fe_3C/N-CNF@RGO-0.1 and Fe_3C/N-CNF@RGO-0.4 electrodes at a rate of 2 C.

(a)

(b)

Fig. S13 The picture of separator state of (a) N-CNF and (b) Fe_3C/N-CNF@RGO-0.2 of LSBs after cycling

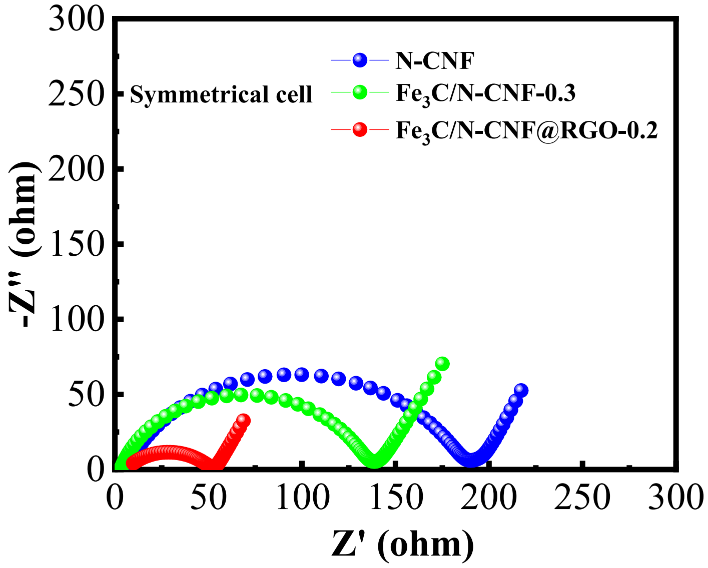

Fig. S14 EIS spectra of the symmetric cells with N-CNF, Fe_3C/N-CNF-0.3 and Fe_3C/N-CNF@RGO-0.2.

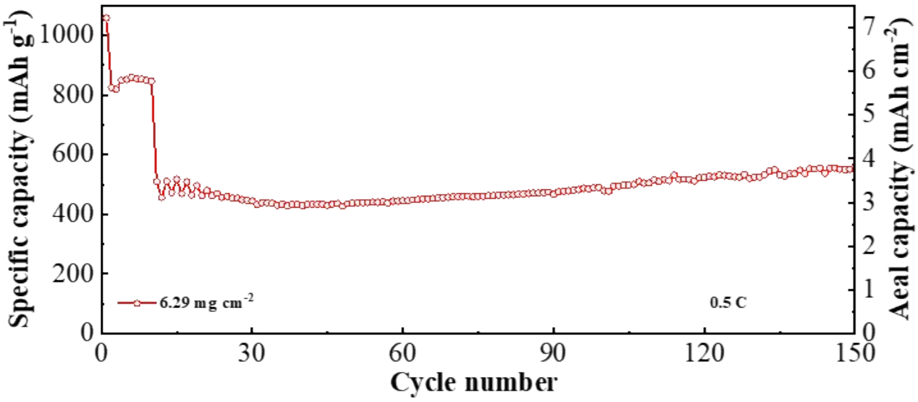

Fig. S15 Cycling stability of the Fe_3C/N-CNF@RGO-0.2 electrode at 0.5 C for 150 cycles with a high sulfur loading of 6.29 mg cm^{-2} after activating at 0.2 C for 10 cycles.

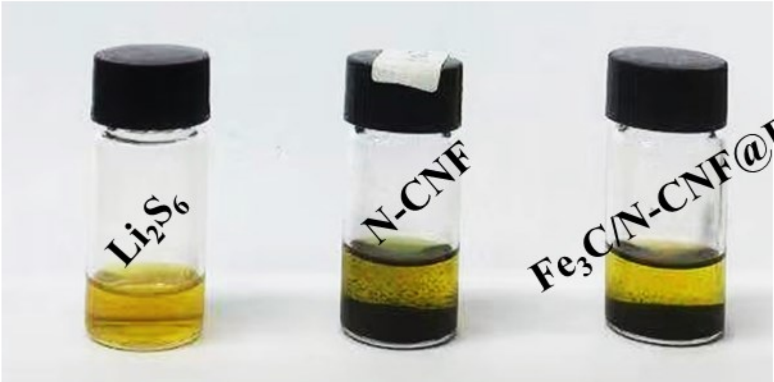

Fig. S16 Visual adsorption observation of Li_2S_6 on the N-CNF and Fe_3C/N-CNF@RGO-0.2 composites at original state.

Table S1

Comparation of the long-cycling capacity decay rate per cycle of Fe_3C/N-CNF@RGO-0.2 with the reported literatures

Sample	Current intensity	Cycle	Capacity decay rate per cycle	Specific Capacity (mA h g $^{-1}$)	Sulfur loading (mg cm $^{-2}$)	Reference
Fe_3C/N-CNF@RGO-0.2	0.5 C	300	0.0089%	781.4	1.62	**This work**
Co−Fe−P nanocubes	1 C	500	0.043%	678	1	[1]
MXene/rGO aerogel	1 C	500	0.07%	596	1.57	[2]
Fe_3C@NPCS-S	0.5 C	300	0.135%	676	1.5	[3]
Fe_3C@N–C/S	0.5 C	400	0.08%	586	1.5	[4]
Fe_3C/OMMC-S NSs	1 C	1000	0.033%	700	1	[5]
HG/LFP/S	1 C	500	0.044%	831	4.3	[6]
Fe_3C-MC	0.5 C	1000	0.037%	920	1.5	[7]
Fe_2O_3–Fe_3C heterostructure	1 C	300	0.037%	776.2	1.3	[8]
CMS900	1 C	200	0.16%	443	1.6	[9]

Reference

S1 Y. Chen, W. X. Zhang, D. Zhou, H. J. Tian, D. W. Su, C. Y. Wang, D. Stockdale, F. Y. Kang, B. H. Li, G. X. Wang, ACS Nano, 2019, 13, 4731-4741.

S2 J. J. Song, X. Guo, J. Q. Zhang, Y. Chen, C. Y. Zhang, L. Q. Luo, F. Y. Wang, G. X. Wang, Journal of Materials Chemistry A, 2019, 7, 6507-6513.

S3 Y. Z. Wang, M. Li, L. C. Xu, T. Y. Tang, Z. Ali, X. X. Huang, Y. L. Hou, S. Q. Zhang, Chemical Engineering Journal, 2019, 358, 962-968.

S4 H. Y. Zhang, H. T. Cui, J. Li, Y. Y. Liu, Y. Z. Yang, M. R. Wang, Nanoscale, 2019, 11, 21532-21541.

S5 Z. S. Jin, M. Zhao, T. N. Lin, Z. Wang, Q. Zhang, B. Q. Liu, L. Li, L. H. Chen, L. Y. Zhang, Z. M. Su, C. G. Wang, Chemical Engineering Journal, 2020, 388, 124315.

S6 B. Wang, F. Jin, Y. Xie, H. Luo, F. Wang, T. T. Ruan, D. L. Wang, Y. Zhou, S. X. Dou, Energy Storage Materials, 2020, 26, 433-442.

S7 H. X. Li, S. Ma, H. Q. Cai, H. H. Zhou, Z. Y. Huang, Z. H. Hou, J. J. Wu, W. J. Yang, H. B. Yi, C. P. Fu, Y. F. Kuang, Energy Storage Materials, 2019, 18, 338-348.

S8 Z. Cao, J. Jia, S. Chen, H. Li, M. Sang, M. Yang, X. Wang, S. Yang, ACS Appl Mater Interfaces, 2019, 11, 39772-39781.

S9 S. Li, Q. Xiang, M. K. Aslam, Y. Cen, C. Z. Guo, J. H. Hu, W. Li, C. G. Chen, Journal of Electroanalytical Chemistry, 2019, 850, 113408